Metabolic dynamics analysis by massive data integration: application to tsunami-affected field soils in Japan

Tatsuki Ogura [1, 2], Yasuhiro Date [1, 2], Yuuri Tsuboi [1], and Jun Kikuchi [1, 2, 3, *]

[1]RIKEN Center for Sustainable Resource Science, 1-7-22 Suehiro-cho, Tsurumi-ku, Yokohama 230-0045, Japan

[2]Graduate School of Medical Life Science, Yokohama City University, 1-7-29 Suehiro-cho, Tsurumi-ku, Yokohama 230-0045, Japan

[3]Graduate School of Bioagricultural Sciences, Nagoya University, 1 Furo-cho, Chikusa-ku, Nagoya 464-0810, Japan

*Corresponding author:

Jun Kikuchi

RIKEN Center for Sustainable Resource Science

1-7-22 Suehiro-cho, Tsurumi-ku, Yokohama 230-0045, Japan

Phone: +81455039490;

Fax: +81455039489;

E-mail:jun.kikuchi@riken.jp

Supplementary Text

RESULTS AND DISCUSSION

Chemical Characterization of Plant Biomass. The chemical compositions of soybean haulms, tomato haulms, and komatsuna leaves were characterized using ^{1}H-^{13}C heteronuclear single quantum coherence (HSQC) and HSQC-total correlation spectroscopy (HSQC-TOCSY) (Supplementary Figure S2 and Supplementary Table S1). The components detected in the HSQC spectra for each plant sample were annotated using SpinAssign (http://prime.psc.riken.jp/)[1–3] and confirmed using HSQC-TOCSY spectra (Table S1). The main components of the soybean haulms were butyrate, lactate, L-aspartate, and some saccharides (i.e., D-glucose, D-xylose, and maltose). Tomato haulms contained these components as well as ethanol, D-fructose, L-asparagine, and L-valine. Komatsuna leaves were characterized by high signal levels for L-glutamate and cytidine but not D-mannose. These components were more abundant in tomato haulms and komatsuna leaves than in soybean haulms, whereas komatsuna leaves exhibited a higher chemical diversity.

Metabolic and Microbial Community Profiling Using an Integrated Approach. Experiments on biomass degradation by the soil microbial community were conducted to characterize the metabolic dynamics in the degradation process of three types of plant biomass using ^{1}H- and ^{13}C-NMR metabolic profiling. First, ^{1}H-NMR metabolic profiling revealed that the profiles were likely to be clustered according to differences in plant composition and based on specific metabolites such as acetate and ethanol (Supplementary Figure S3A and S3B). While these metabolites characterized the metabolic dynamics of each plant in the degradation process, the

detailed saccharide degradation process could not be identified from this profile because of overlapping signals of each saccharide compound in the ^{1}H-NMR spectra. Therefore, ^{13}C-NMR profiling was performed to enhance the resolution of the saccharide regions. The ^{13}C-NMR spectra revealed that the profiles were clustered according to differences in the input sources from each plant, and individual saccharides, such as D-xylose and D-galacturonate, amino acids, and SCFAs, such as acetate, lactate, and valine were all plainly visible (Supplementary Figure S3C and S3D).

Metabolic Profiles of Three Types of Plant Biomass Characterized by Integrated Analysis Based on ^{1}H- and ^{13}C-NMR Data. ^{1}H- and ^{13}C-NMR data were integrated and analyzed using PCA. The metabolic profiles reflected each degradation process in the score plot (Supplementary Figure S3E). Many signals contributing to the separation were identified in the associated loading plots (Supplementary Figures S3F and S3G). In the score plot, all three degradation processes shifted from PC1 negative to positive during plant degradation. In contrast, PC2 directionality was found to identify a specific characteristic of the degradation process for each plant. From Day 1 to 22, the degradation profile of the soybean samples shifted in the PC2 positive direction, whereas that of the komatsuna samples shifted in the PC2 negative direction. The ^{1}H- and ^{13}C-NMR loading plots from the integrated analysis showed that acetate contributed to the PC1 positive shift and that acetate was generated during the degradation process. In PC2, lactate contributed to the positive shift, whereas ethanol, butyrate, and choline drove the negative shift. These data indicate that lactate predominantly contributed to soybean degradation and that ethanol, butyrate, and choline dominated during komatsuna degradation. Moreover, few saccharide signals contributed to the positive shift, suggesting that they were consumed by soil

microbiota to generate other organic compounds, such as acetate and lactate (soybean degradation process) or acetate, ethanol, and butyrate (komatsuna degradation process). These data suggest that each plant biomass possesses distinct metabolic dynamics during degradation based on their complex chemical composition.

Time-course Variations of Metabolic Profiles in Plant Degradation Processes. The three types of plant biomass were incubated with the soil microbial community, and their degradation profiles were monitored over 22 days (Supplementary Figures S3H–S3J). In soybean, saccharide compounds were rapidly degraded from Day 1 to 4 during acetate, lactate, and butyrate production. Acetate accumulation continued until Day 22, whereas butyrate was produced exponentially until Day 6. Lactate accumulated rapidly until Day 3, maintained a steady concentration until Day 11, then decreased until Day 22. In tomato, saccharides and L-asparagine were slightly degraded from Day 1 to 11, while acetate, lactate, propionate, and ethanol were produced. The accumulation of acetate, lactate, and propionate continued until Day 22, whereas ethanol was produced very rapidly from Day 1 to 3. In komatsuna, D-fructose was degraded from Day 1 to 6, whereas acetate, lactate, propionate, butyrate, L-valine, L-arginine, and L-asparagine were produced. Acetate, propionate, L-valine, and L-arginine continued to accumulate from Day 1 to 22, and lactate was produced from Day 1 to 10. Low levels of butyrate were detected starting from Day 8. Taken together, these data show that the degradation of the three types of biomass by soil microbiota was characterized by the consumption of saccharide components and the accumulation of organic acids and amino acids. Detailed analysis of the metabolic products and their dynamics revealed distinct degradation processes for each plant biomass.

Time-course Variations of Microbiota Profiles in Plant Degradation Processes. The impact of plant biomass degradation on the microbiota was determined by pyrosequencing analysis in combination with PCA (Supplementary Figure S4). The PCA score plot shows that the microbiota profiles of all three types of plant biomass shifted from PC1 negative to positive during the degradation process. Soybean samples contained distinct microbiota during Days 1–3 and Days 4–22. The microbiota of the tomato samples was more dynamic, with significant changes during Days 1–3, Days 4–6, and Days 8–22. In contrast, komatsuna samples changed gradually from Day 1 to 22. The loading plot analysis revealed that *Lactobacillus* sp. contributed to the PC1 positive shift, indicating that this bacterium became the dominant species in the microbiota during plant degradation. For PC2, *Pediococcus* sp. contributed to the negative shift, which acted strongly on Days 4–6 of the tomato degradation process. In addition, time-course analysis confirmed that *Lactobacillus* sp. became the major bacterium in all three types of biomass within 3–6 days of degradation (Supplementary Figures S4K‑S4M). However, the transitions in the microbiota composition over time differed among plants. In soybean plants, *Pseudomonas* sp. and *Klebsiella* sp. originally dominated but decreased drastically in number within 3 days. *Lactococcus* sp. was most abundant on Days 2–3, then practically disappeared over the following week as *Lactobacillus* sp. became dominant. In tomato plants, *Pediococcus* sp. dominated during the first 6 days, then their numbers decreased. In komatsuna, *Klebsiella* sp. and *Trabulsiella* sp. were the major bacteria in the early stage and only slightly decreased during the degradation process. In contrast, *Pediococcus* sp. became more abundant from Day 1 to 5 and gradually decreased, finally disappearing on Day 9. Taken together, these time-course analyses demonstrate that each type of plant biomass has a different effect on the microbiota composition

during degradation. Thus, each type of plant generates a unique local microbiota and chemical environment, which evolve together during the degradation process.

Correlation Analysis between Metabolites and Bacteria during Biomass Degradation. Correlation analysis was performed to reveal the relationships between metabolic dynamics and microbial transitions during biomass degradation (Supplementary Figures S5 and S6). A positive correlation between the levels of a metabolic product and a bacterium indicates that this bacterium was involved in the production of the metabolite. In contrast, a negative correlation between the levels of a specific saccharide and a bacterium indicates that this bacterium consumed the saccharide. In soybeans, positive correlations were observed between acetate and *Lactobacillus* sp., lactate and *Pediococcus* sp., and pyruvate and *Lactobacillus* sp. Negative correlations were observed between saccharides (D-xylose, D-fructose, and D-galactose) and *Lactobacillus* sp. In tomatoes, positive correlations were observed for acetate and ethanol with *Lactobacillus* sp., and between L-aspartate and *Lactococcus* sp., *Klebsiella* sp., and *Serratia* sp. In contrast, negative correlations were observed between saccharides (D-fructose and D-xylose) and *Lactobacillus* sp., between D-mannose and *Erwinia* sp., *Trabulsiella* sp., *Yersinia* sp., and *Pseudomonas* sp., and between L-asparagine and *Pediococcus* sp. In komatsuna, positive correlations were observed between several compounds (i.e., lactate, acetate, butyrate, L-arginine, L-leucine, L-valine, and pyruvate) and *Lactobacillus* sp., and between L-aspartate and *Yersinia* sp. In contrast, negative correlations were observed between saccharides (D-fructose, D-galactose, and D-glucose) and *Lactobacillus* sp.. This analysis established the relationships between degraded saccharide compounds, metabolic products, and specific bacteria.

Evaluation of Plant Degradation Pathways. Using this approach, we identified the metabolic pathways supported by the key bacteria responsible for metabolic dynamics during biomass degradation (Supplementary Figure S6). In these pathways, *Lactobacillus* and *Pediococcus* sp. are referred to as "lactic acid bacteria", because they are responsible for lactate production: member species include *L. brevis*, *L. buchneri*, and *P. dextrinicus*.[4,5] Other metabolic functions have also been reported for these species, such as ethanol production from glucose by *L. brevis*[4] and acetate production from lactate by *L. buchneri*.[6] Because the "lactic acid bacteria" detected in this study are taxonomically related to these species, they are likely to support acetate, lactate, and ethanol production.

METHODS

^{13}C-Labeled Plant Biomass Samples. Three types of plant biomass samples were used in this study: soybean haulms, tomato haulms, and komatsuna leaves (Japanese Mustard Spinach, *Brassica rapa* var. *viridis*), grown in an acrylic chamber filled with $^{13}CO_2$ gas at 340 ppm. The detailed experimental procedure for the production of these ^{13}C-labeled plant samples has been reported in a previous study.[23]

Sample Preparation. Lyophilized ^{13}C-labeled samples were processed as food milling (FM) samples in a blender. The samples were further ground using a planetary ball milling (BM) machine (Fritsch Japan Co., Ltd., Kanagawa, Japan). In the preparation of the BM samples, approximately 300–400 mg of each FM sample was loaded into ZrO_2 pots (12 ml inner volume) with 50 ZrO_2 ceramic balls (5 mm diameter), and processed at 400 rpm for 6 h to generate 5 g of material.

PCR-DGGE. For the PCR-DGGE analysis, each DNA sample was amplified by PCR using universal bacterial primers specific for the V6–V8 regions of the 16S rRNA genes of the domain Bacteria: 968f-gc (5′-CGC CCG GGG CGC GCC CCG GGC GGG GCG GGG GCA CGG GGG GAA CGC GAA GAA CCT TAC-3′) and 1368r (5′-CGG TGT GTA CAA GGC CCG GGA ACG-3′).[7] Each reaction mixture contained 10 pmol of each primer, 0.16 mM of deoxyribonucleoside triphosphate, 25 µl of 2× KOD FX Neo buffer, 1.25 U of KOD FX Neo polymerase (Toyobo Co. Ltd., Japan), and sterilized water added to a final volume of 50 µl. Touchdown PCR was performed to reduce spurious PCR products. After a melting step (95 °C; 4 min), PCR cycles of denaturing (95 °C; 30 s), annealing (61–56 °C; 30 s), and elongation (72 °C; 1 min) were performed with 10 cycles where annealing temperature decreased by 0.5 °C every other cycle and with 20 subsequent cycles using a 56 °C annealing temperature, followed by extension at 72 °C for 10 min.

Standard polyacrylamide gel electrophoresis conditions were used as have been described previously.[8] The DGGE gels were stained with SYBR Green I (Lonza, Rockland, ME, USA), and images were acquired using the GelDoc XR system (Bio-Rad Laboratories Inc., Tokyo, Japan). DGGE images were analyzed using Quantity One software (Bio-Rad). Signal intensities and band positions in each lane were divided into a spectrum of 100 variables, and the data were preprocessed for statistical analysis using a method reported previously.[9]

SUPPLEMENTARY FIGURE LEGENDS

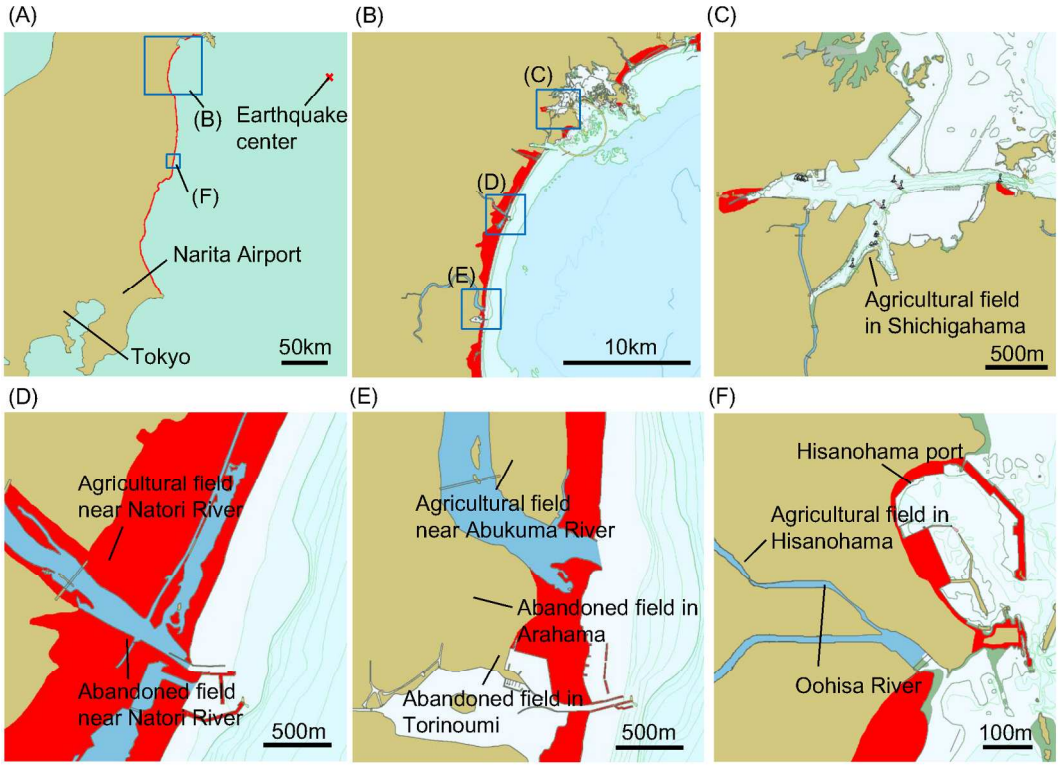

Figure S1. Maps of the tsunami disaster area caused by the Great East Japan earthquake in 2011. Figures show the national map of Japan (A), Miyagi Prefecture (B), Shichigahama region (C), Natori River region (D), Abukuma River region (E). and Hisanohama region (F). Red-colored regions indicate the disaster area where the tsunami reached over 4 m in height. Figures were obtained from the International Research Institute of Disaster Science (http://michinoku.irides.tohoku.ac.jp/ttjt/ttjt_view.html).

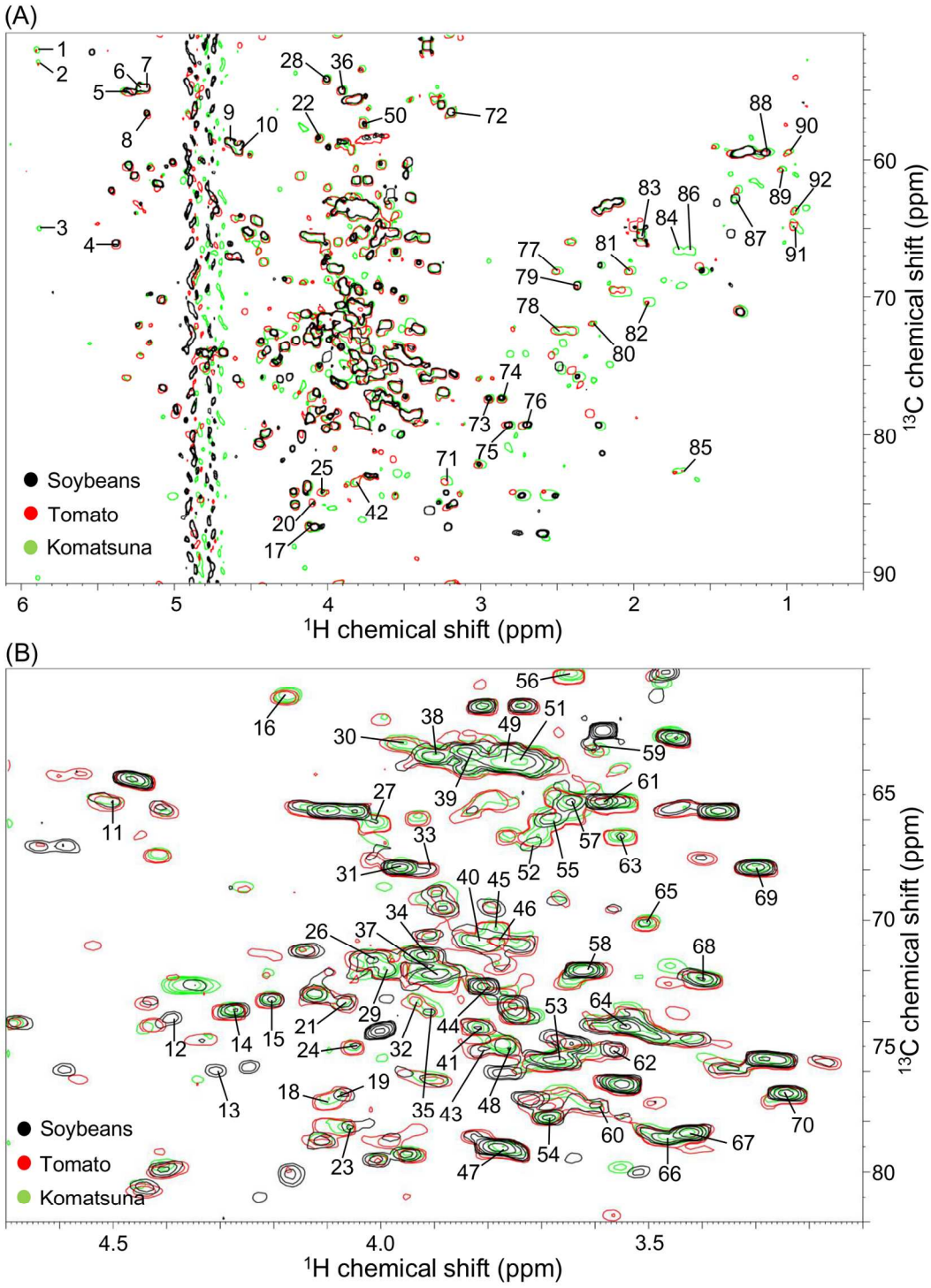

Figure S2. ^{1}H-^{13}C HSQC NMR spectra for biomass samples of soybean haulms, tomato haulms, and komatsuna leaves. (A) The region from 0.5 to 6.1 ppm corresponds to ^{1}H and that from 50 to 90 ppm corresponds to ^{13}C. (B) The saccharide region from 3.1 to 4.7 ppm corresponds to ^{1}H and

that from 60 to 82 ppm corresponds to ^{13}C. Black, red, and green denote soybean, tomato, and komatsuna samples, respectively. Numbers indicate annotated metabolites listed in Supplementary Table S1.

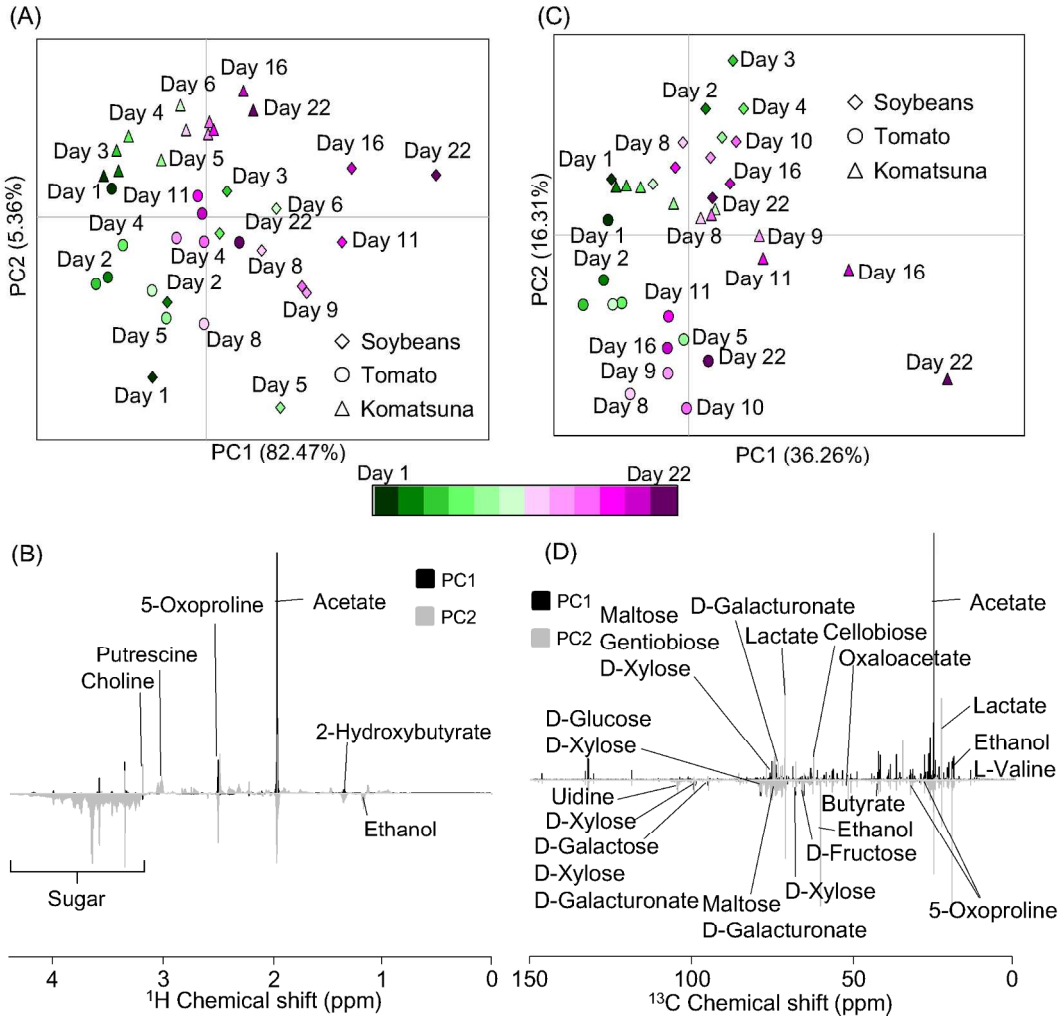

Figure S3. Metabolic profiles from ^{1}H-NMR (A and B), ^{13}C-DEPT NMR (C and D), and integrated analysis (E–G). PCA score plots (A, C and E) and loading plots (B, D, F and G) based on the results of each analytical method are shown. Time-course variations of the molecules detected during the plant biomass degradation experiments are shown for soybean (H), tomato (I), and komatsuna (J).

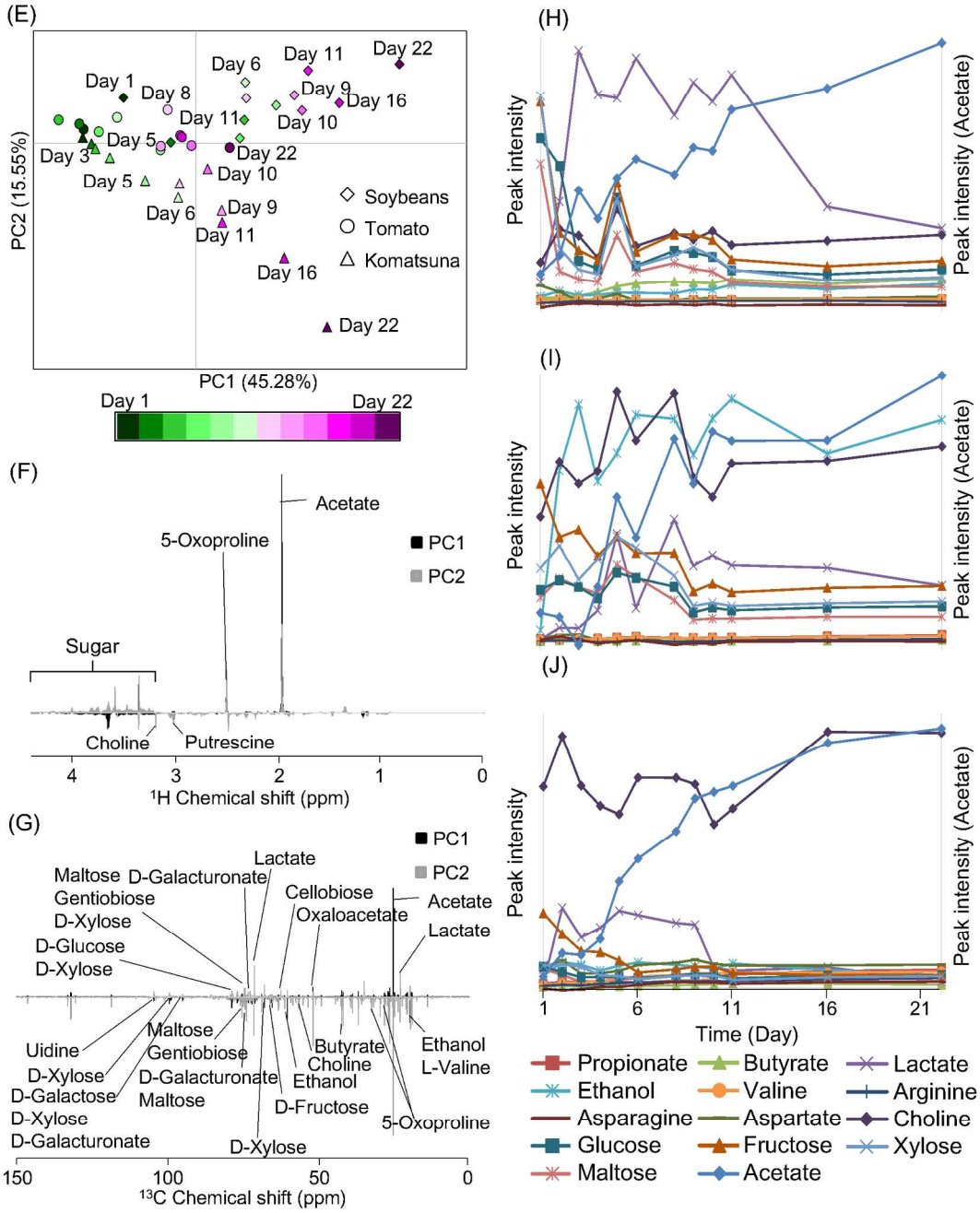

Figure S3. continued

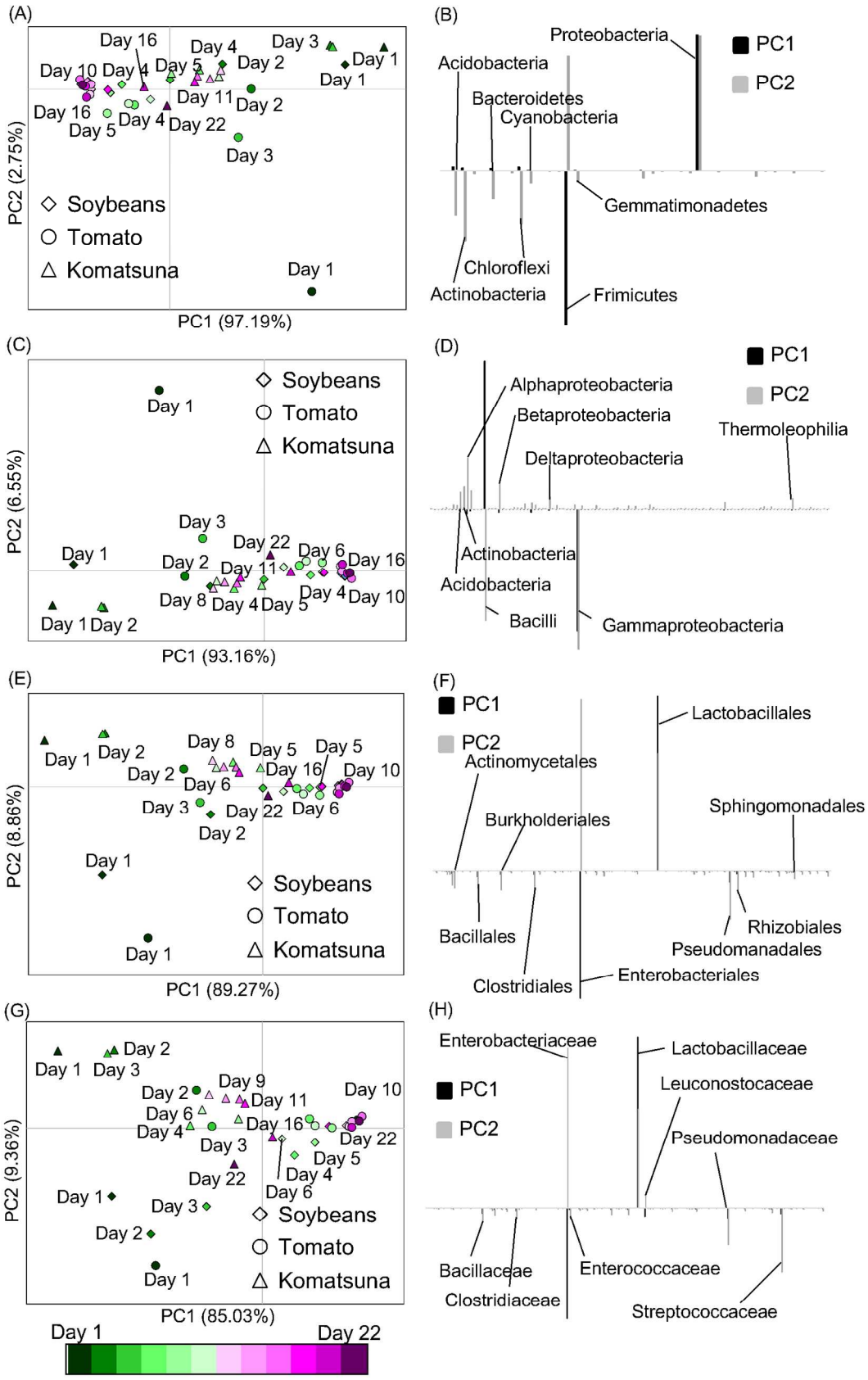
(A)
PC2 (2.75%)
PC1 (97.19%)
Soybeans
Tomato
Komatsuna
(B)
PC1
PC2
Proteobacteria
Acidobacteria
Bacteroidetes
Cyanobacteria
Gemmatimonadetes
Chloroflexi
Actinobacteria
Frimicutes
(C)
PC2 (6.55%)
PC1 (93.16%)
Soybeans
Tomato
Komatsuna
(D)
PC1
PC2
Alphaproteobacteria
Betaproteobacteria
Thermoleophilia
Deltaproteobacteria
Actinobacteria
Acidobacteria
Bacilli
Gammaproteobacteria
(E)
PC2 (8.86%)
PC1 (89.27%)
Soybeans
Tomato
Komatsuna
(F)
PC1
PC2
Lactobacillales
Actinomycetales
Sphingomonadales
Burkholderiales
Bacillales
Rhizobiales
Pseudomanadales
Clostridiales
Enterobacteriales
(G)
PC2 (9.36%)
PC1 (85.03%)
Soybeans
Tomato
Komatsuna
Day 1
Day 22
(H)
Enterobacteriaceae
Lactobacillaceae
Leuconostocaceae
PC1
PC2
Pseudomonadaceae
Bacillaceae
Enterococcaceae
Clostridiaceae
Streptococcaceae

1

Figure S4. Microbiota profiles in the biomass degradation process (A–J). PCA score plots (A, C, E, G and I) and loading plots (B, D, F, H and J) are divided according to taxonomic level: phylum (A and B), order (C and D), class (E and F), family (G and H), and genus (I and J). Time-course variations of the microbiota in the biomass degradation process are shown for soybean (K), tomato (L) and komatsuna (M).

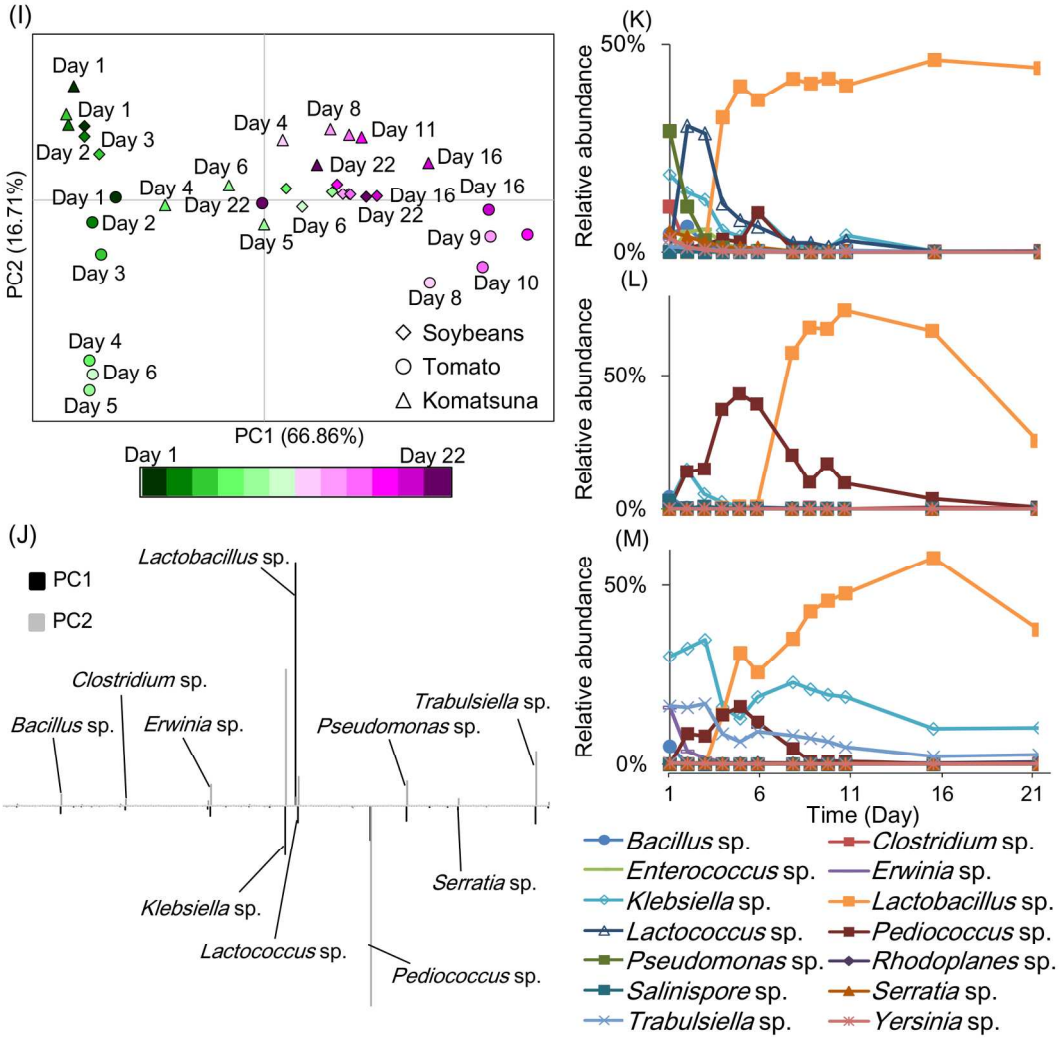

Figure S4. continued

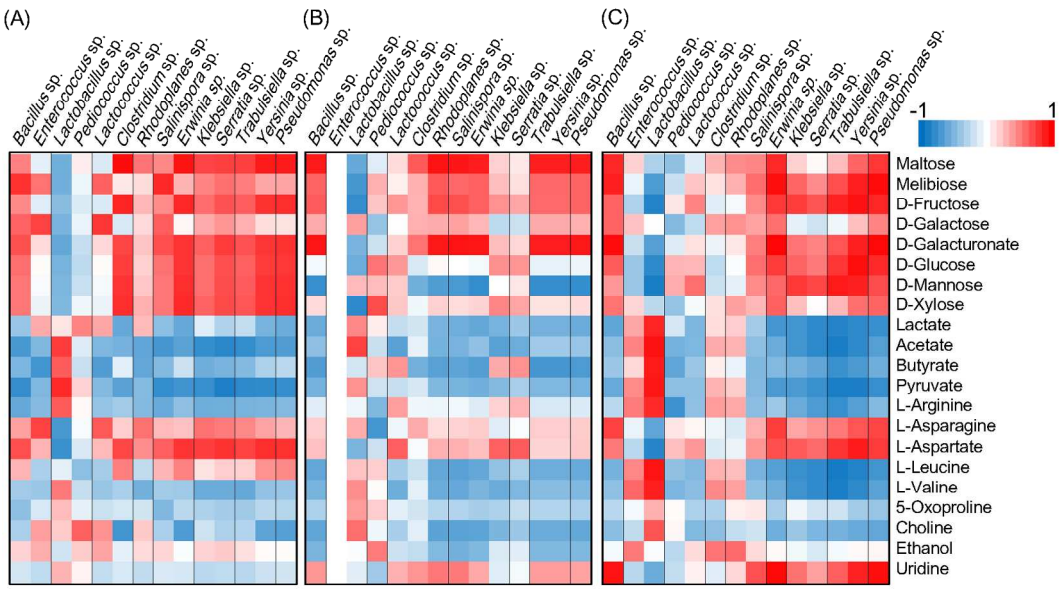

Figure S5. Correlation analysis of time-course variations between metabolites and soil microbiota obtained from NMR and pyrosequencing analysis. Two-dimensional correlation maps for soybean haulms (A), tomato haulms (B), and komatsuna leaves (C) are displayed. Red and blue denote positive and negative correlations, respectively.

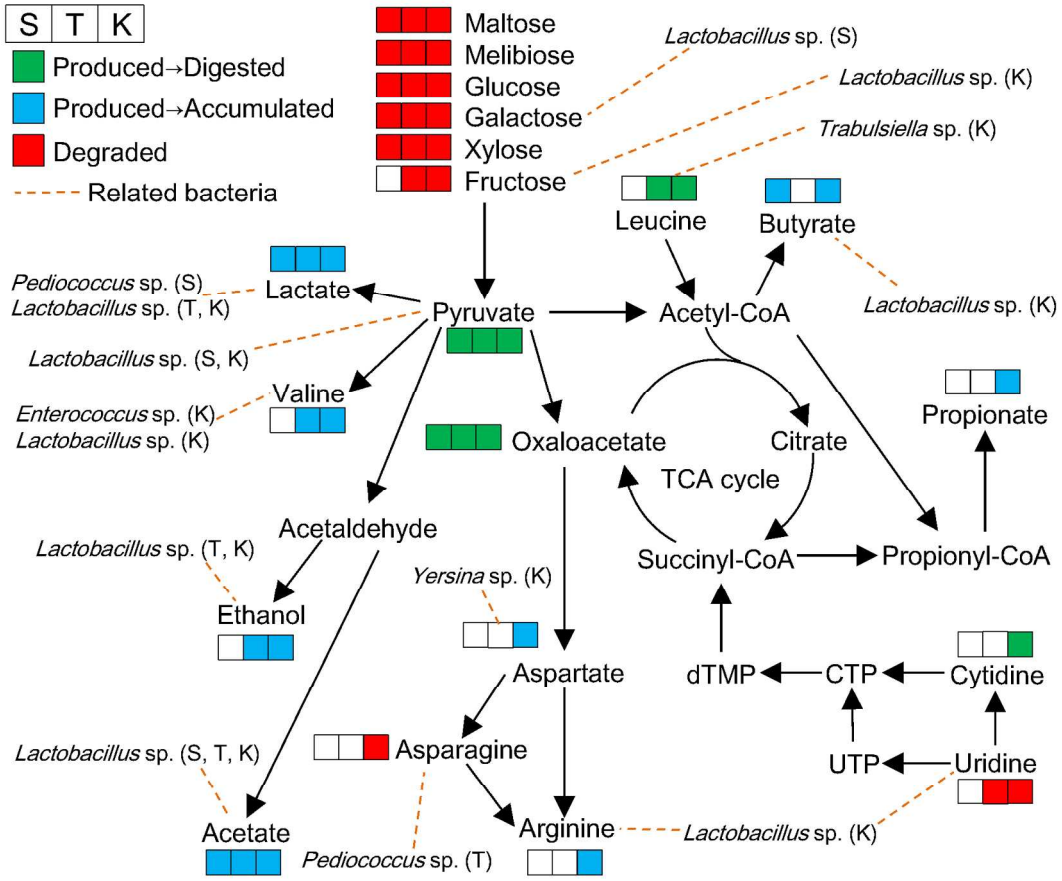

Figure S6. Deduced metabolic pathways mediated by different microbiota supporting each step of the plant biomass degradation process. Red, green, and blue boxes denote degraded, produced and then degraded, and produced and finally accumulated components, respectively. Dashed lines indicate relationships between metabolite degradation/production and the bacteria responsible based on correlation analysis. S; soybean haulms, T; tomato haulms, K; komatsuna leaves.

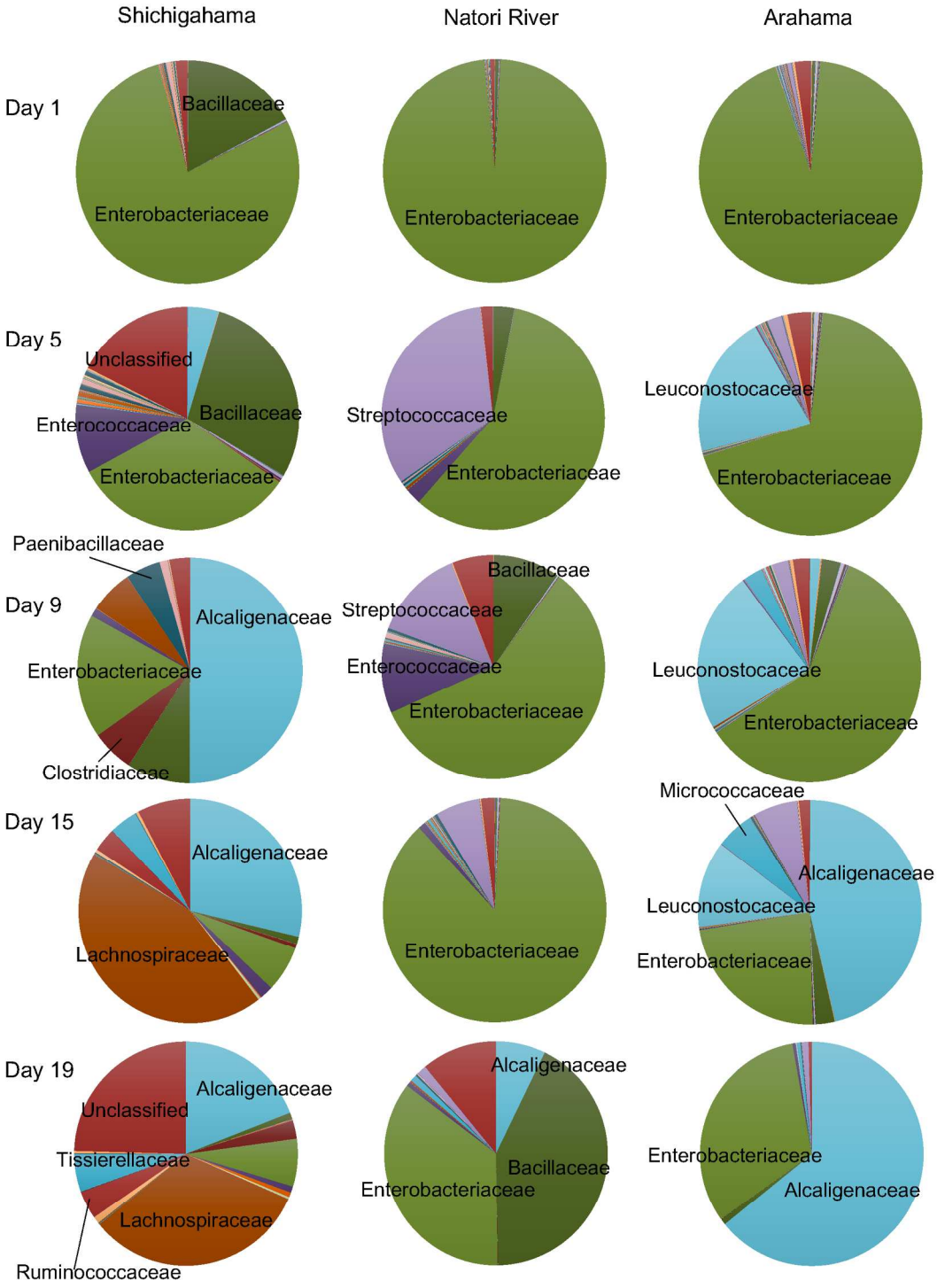

Figure S7. Comparisons of microbiota profiles at the family level in the komatsuna degradation process in the soil of three fields.

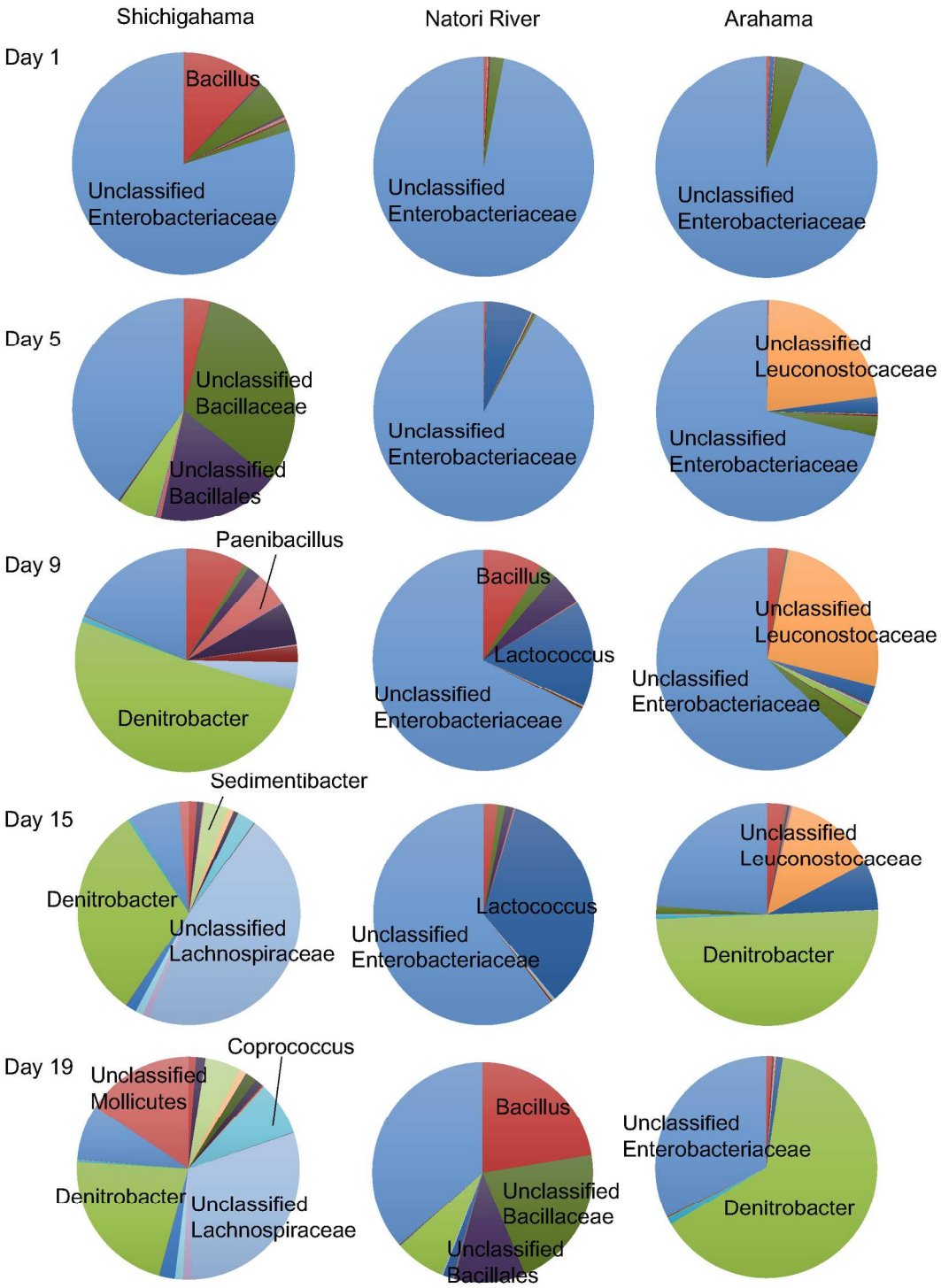

Figure S8. Comparisons of microbiota profiles at the genus level in the komatsuna degradation process in the soil of three fields.

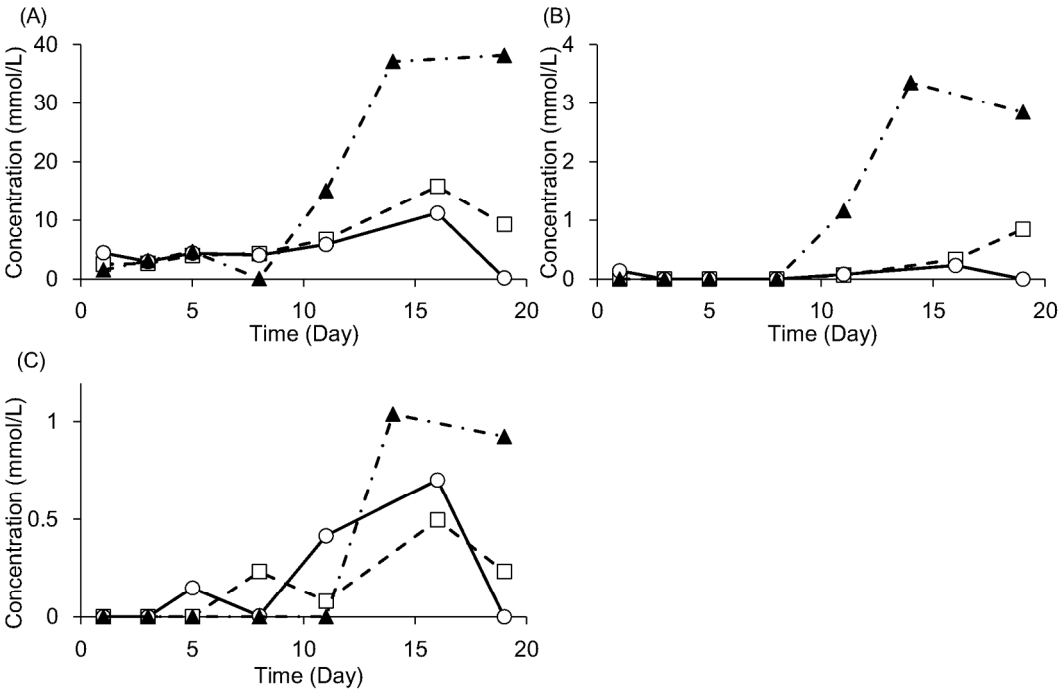

Figure S9. Time course changes of each SCFA. The metabolites are acetate (A), propionate (B), butyrate (C), respectively. Symbols represent an agricultural field in Shichigahama (closed triangle), an abandoned field near the Natori River (open square), and an abandoned field in Arahama (open circle).

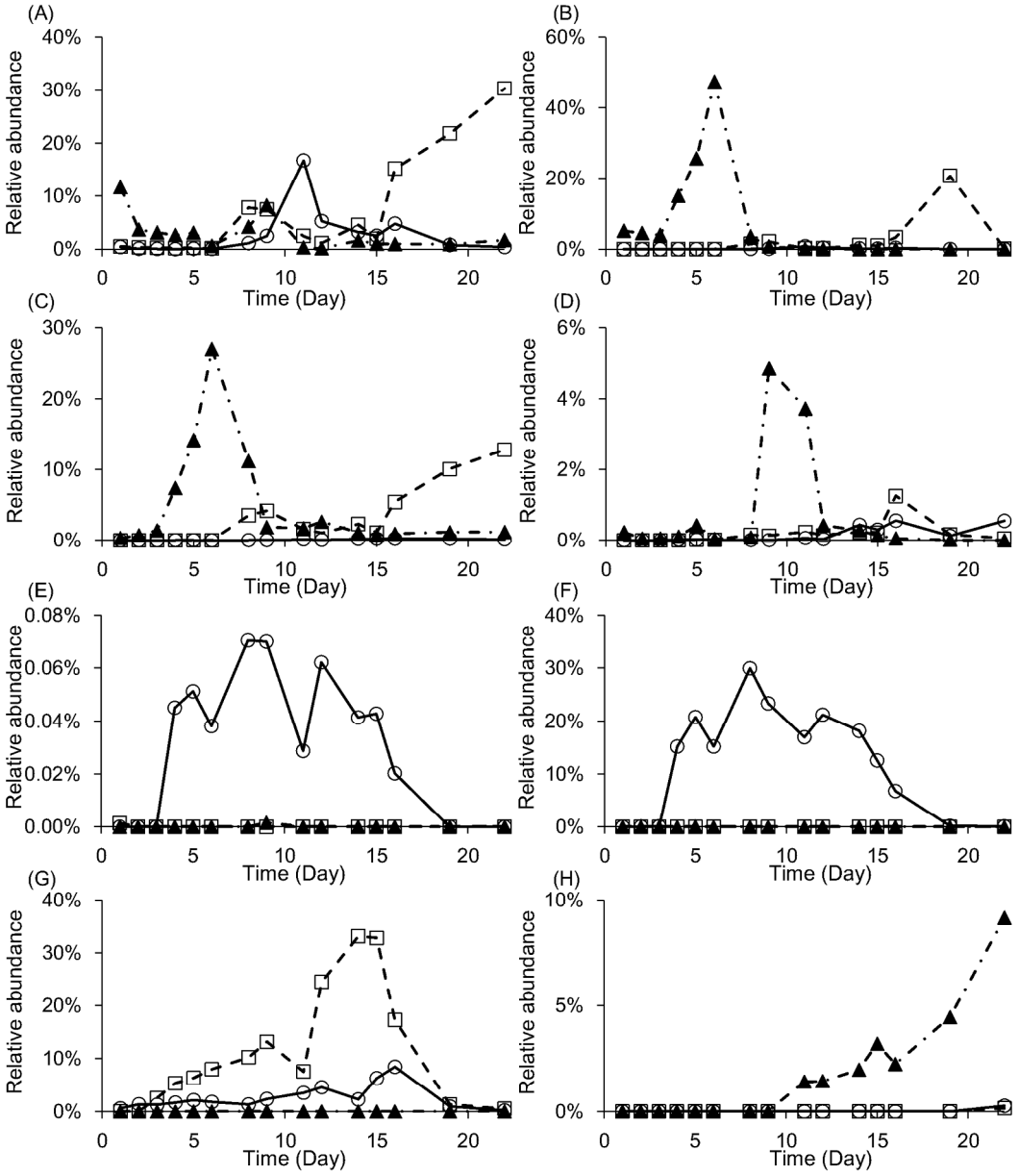

Figure S10. Dynamics of the relative abundance of bacteria in the biomass degradation process. *Bacillus* sp. (A), unclassified Bacillaceae (B), unclassified Bacillales (C), *Paenibacillus* sp. (D), *Weissella* sp. (E), unclassified Leuconostocaceae (F), *Lactococcus* sp. (G), *Sedimentibacter* sp. (H), Clostridium sp. (I), *Coprococcus* sp. (J), unclassified Lachnospiraceae (K), *Denitrobacter* sp. (L), *Pantoea* sp. (M), unclassified Enterobacteriaceae (N), and unclassified Mollicutes (O).

Symbols represent an agricultural field in Shichigahama (closed triangle), an abandoned field near the Natori River (open square), and an abandoned field in Arahama (open circle).

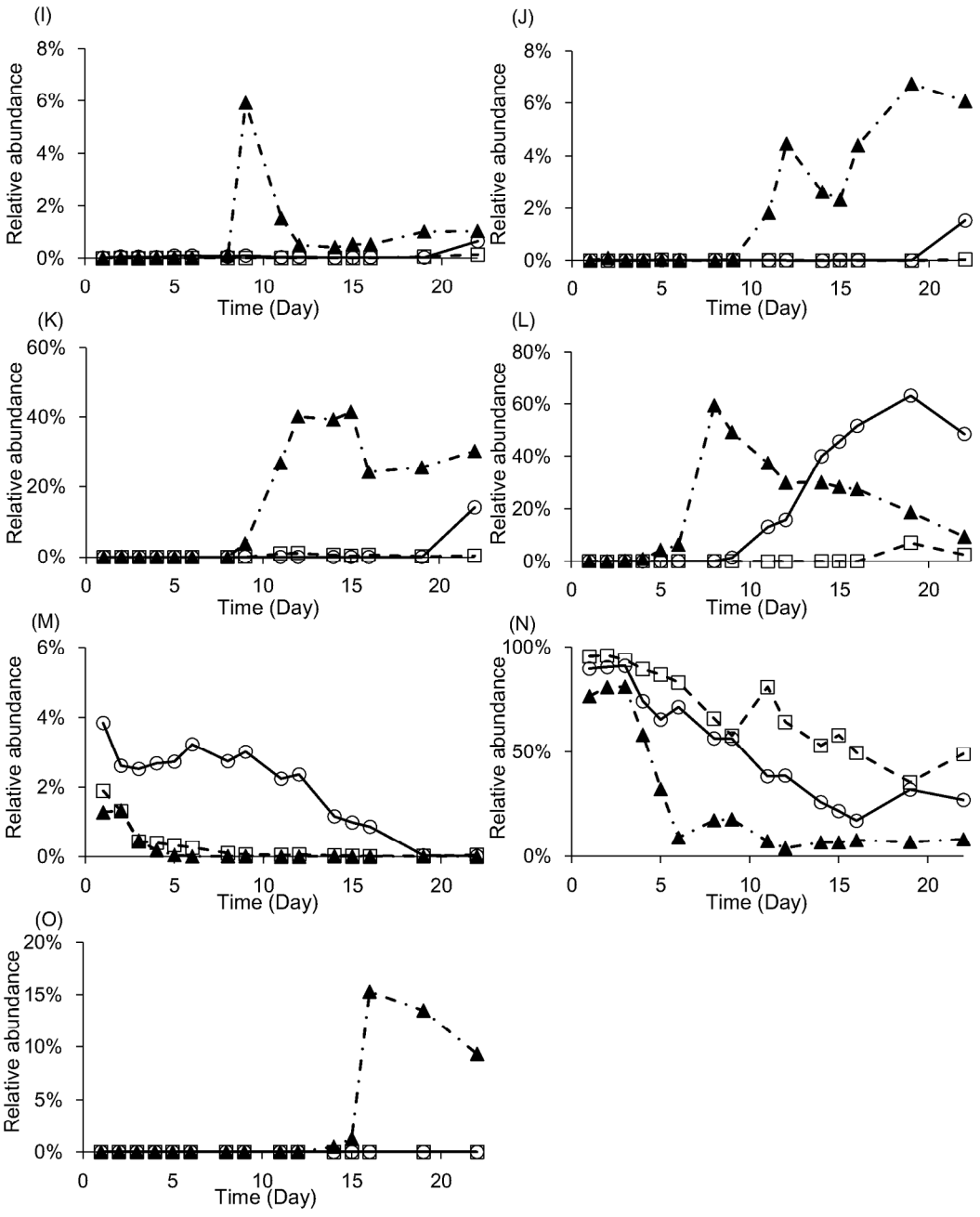

Figure S10. continued

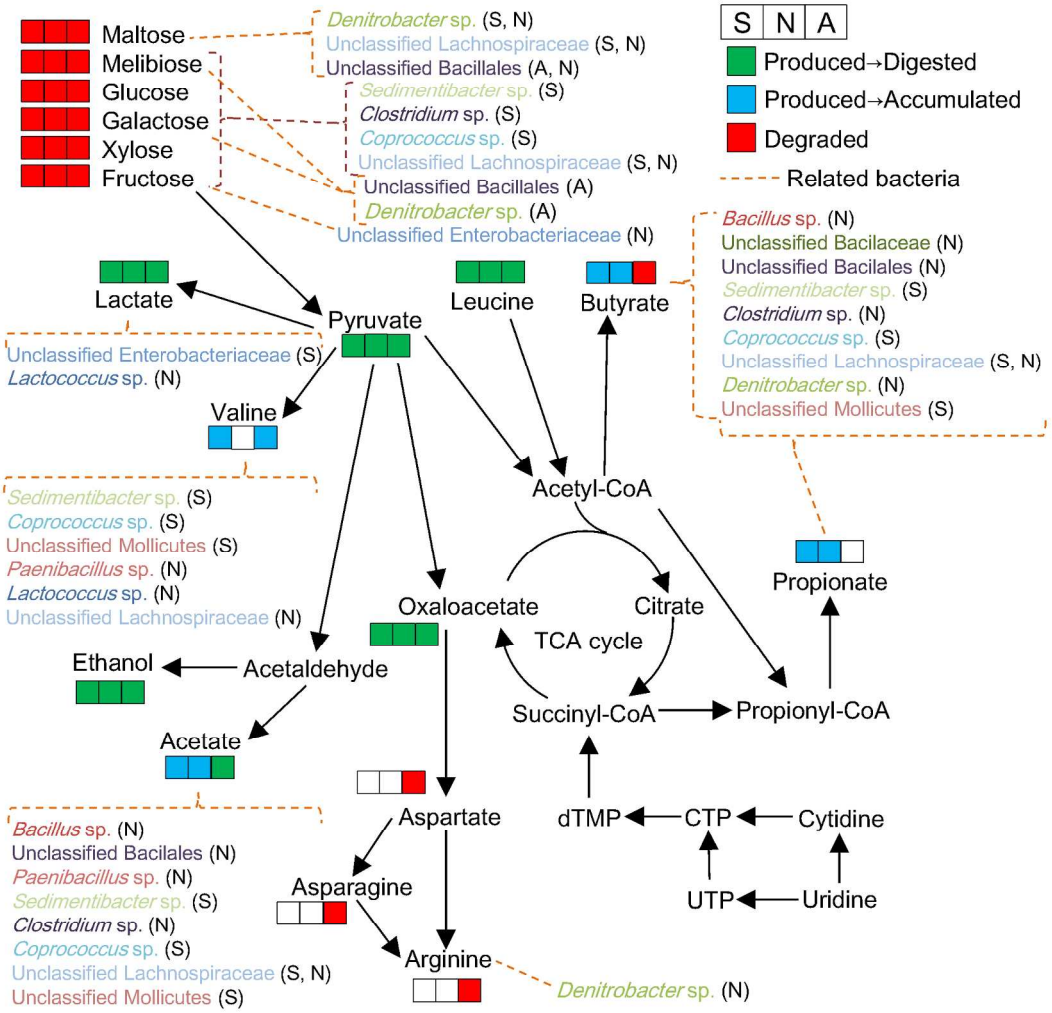

Figure S11. Deduced metabolic pathways for each step of the plant biomass degradation process annotated with the subpopulations of the microbial community supporting each step. Red, green, and blue boxes denote degraded, produced and then degraded, and produced and finally accumulated components, respectively. The dashed lines indicate relationships between metabolite degradation/production and the responsible bacteria based on correlation analysis. S; agricultural field in Shichigahama, N; abandoned field near the Natori River, and A; abandoned field in Arahama.

1

Table

Table S1. Annotation list of HSQC spectra

	δ_H (ppm)	δ_C (ppm)	Annotation			
1	5.91	52.09	Uridine			
2	5.90	52.83	Cytidine			
3	5.89	65.01	Uridine			
4	5.38	66.01	Maltose			
5	5.27	55.08	D-Galactose	D-Galacturonate		
6	5.23	54.73	α-Glucose	Cellobiose	D-Glucuronate	Gentiobiose
			Melibiose			
7	5.19	54.76	D-Xylose			
8	5.18	56.59	D-Mannose			
9	4.64	58.63	β-Glucose	Cellobiose	D-Glucuronate	Gentiobiose
			Melibiose			
10	4.58	59.22	D-Galactose	D-Galacturonate	D-Xylose	
11	4.51	65.21	Cellobiose	Gentiobiose		
12	4.39	73.82	D-Galacturonate			
13	4.31	75.92	Uridine			
14	4.27	73.51	D-Galacturonate			
15	4.20	73.10	D-Galacturonate			
16	4.18	61.06	5-Oxoproline			
17	4.12	86.53	Cytidine	Uridine		
18	4.10	77.21	D-Fructose			
19	4.10	77.05	D-Fructose			
20	4.09	84.95	D-Fructose			
21	4.07	73.20	D-Galactose			
22	4.06	58.32	Choline			
23	4.06	78.13	D-Galacturonate			
24	4.05	74.92	D-Glucuronate			
25	4.03	84.11	D-Fructose			
26	4.02	71.54	D-Fructose			
27	4.01	66.04	D-Fructose			
28	4.00	54.10	L-Asparagine			

29	3.99	71.90	D-Fructose	D-Galactose	Melibiose	
30	3.97	62.86	Cellobiose			
31	3.96	67.86	Melibiose			
32	3.94	73.20	Cellobiose			
33	3.92	67.96	D-Xylose			
34	3.91	71.38	D-Galactose			
35	3.91	73.55	D-Mannose			
36	3.90	54.95	L-Aspartate			
37	3.90	72.12	D-Fructose	D-Galacturonate	D-Mannose	Maltose
			Melibiose			
38	3.90	63.43	β-Glucose	Cellobiose	Cytidine	D-Mannose
			Gentiobiose	Maltose	Uridine	
39	3.84	63.25	α-Glucose	Cellobiose	Cytidine	Maltose
40	3.83	70.81	D-Galactose	D-Fructose	D-Galacturonate	
			Melibiose			
41	3.82	74.12	α-Glucose	Cellobiose		
42	3.82	83.34	D-Fructose			
43	3.82	75.13	D-Mannose			
44	3.81	72.57	D-Mannose			
45	3.79	70.41	D-Fructose			
46	3.79	70.86	D-Galactose			
47	3.78	79.00	Maltose			
48	3.78	74.91	D-Mannose			
49	3.76	63.65	α-Glucose	Cellobiose	D-Galactose	D-Mannose
			Maltose	Melibiose		
50	3.76	57.31	L-Arginine			
51	3.72	63.61	β-Glucose	Gentiobiose		
52	3.72	66.92	D-Fructose			
53	3.69	75.61	α-Glucose	D-Galacturonate	D-Glucuronate	D-Mannose
			D-Xylose	Gentiobiose	Maltose	Melibiose
54	3.68	77.79	D-Galactose			
55	3.68	65.88	D-Fructose			
56	3.65	60.16	Ethanol			
57	3.65	65.26	D-Fructose			
58	3.62	71.93	D-Xylose			
59	3.60	63.27	L-Valine			

60	3.59	77.29	Cellobiose	Gentiobiose	Maltose	
61	3.59	65.23	D-Fructose			
62	3.56	75.19	Maltose			
63	3.55	66.59	D-Fructose			
64	3.54	74.15	α-Glucose	D-Glucuronate		D-Xylose
			Gentiobiose	Maltose	Melibiose	
65	3.51	70.05	Choline			
66	3.47	78.63	β-Glucose	Cellobiose	Gentiobiose	Melibiose
67	3.42	78.40	β-Glucose	D-Xylose		
68	3.40	72.28	α-Glucose	Cellobiose	Gentiobiose	Maltose
69	3.30	67.87	D-Xylose			
70	3.24	76.81	β-Glucose	D-Glucuronate	D-Xylose	Gentiobiose
			Maltose	Melibiose		
71	3.23	83.34	L-Arginine			
72	3.19	56.50	Choline			
73	2.94	77.29	L-Asparagine			
74	2.86	77.30	L-Asparagine			
75	2.81	79.19	L-Aspartate			
76	2.69	79.20	L-Aspartate			
77	2.50	68.09	5-Oxoproline			
78	2.40	72.46	5-Oxoproline			
79	2.37	69.14	Pyruvate			
80	2.27	71.85	L-Valine			
81	2.00	68.10	5-Oxoproline			
82	1.91	70.30	L-Arginine			
83	1.91	66.18	Acetate			
84	1.71	66.72	L-Arginine	L-Leucine		
85	1.68	82.55	L-Leucine			
86	1.64	66.56	L-Arginine			
87	1.33	62.81	Lactate			
88	1.13	59.42	Ethanol			
89	1.03	60.68	L-Valine			
90	0.98	59.36	L-Valine			
91	0.95	64.75	L-Leucine			
92	0.95	63.59	L-Leucine			

1

REFERENCES

1. Chikayama, E., Suto, M., Nishihara, T., Shinozaki, K., Kikuchi, J. (2008) Systematic NMR analysis of stable isotope labeled metabolite mixtures in plant and animal systems: coarse grained views of metabolic pathways. *PLoS One 3*, e3805.

2. Akiyama, K., Chikayama, E., Yuasa, H., Shimada, Y., Tohge, T., Shinozaki, K., Hirai, M. Y., Sakurai, T., Kikuchi, J., Saito, K. (2008) PRIMe: a Web site that assembles tools for metabolomics and transcriptomics. *In Silico Biol. 8*, 339-345.

3. Chikayama, E., Sekiyama, Y., Okamoto, M., Nakanishi, Y., Tsuboi, Y., Akiyama, K., Saito, K., Shinozaki, K., Kikuchi, J. (2010) Statistical indices for simultaneous large-scale metabolite detections for a single NMR spectrum. *Anal. Chem. 82*, 1653-8.

4. Berezina, O. V., Zakharova, N. V., Brandt, A., Yarotsky, S. V., Schwarz, W. H., Zverlov, V. V. (2010) Reconstructing the clostridial n-butanol metabolic pathway in Lactobacillus brevis. *Appl. Microbiol. Biotechnol. 87*, 635-646.

5. Haakensen, M., Dobson, C. M., Hill, J. E., Ziola, B. (2009*) Reclassification of Pediococcus dextrinicus (Coster and White 1964) Back 1978 (Approved Lists 1980) as Lactobacillus dextrinicus comb. nov., and emended description of the genus Lactobacillus. *Int. J. Syst. Evol. Micr. 59*, 615-621.

6. Elferink, S. J. W. H. O., Krooneman, J., Gottschal, J. C., Spoelstra, S. F., Faber, F., Driehuis, F. (2001) Anaerobic conversion of lactic acid to acetic acid and 1,2-propanediol by Lactobacillus buchneri. *Appli. Environ. Microbiol. 67*, 125-132.

7. Heuer, H., Krsek, M., Baker, P., Smalla, K., Wellington, E. M. H. (1997) Analysis of actinomycete communities by specific amplification of genes encoding 16S rRNA and gel-electrophoretic separation in denaturing gradients. *Appl. Environ. Microbiol. 63*, 3233-3241.

8. Date, Y., Nakanishi, Y., Fukuda, S., Kato, T., Tsuneda, S., Ohno, H., Kikuchi, J. (2010) New monitoring approach for metabolic dynamics in microbial ecosystems using stable-isotope-labeling technologies. *J. Biosci. Bioeng. 110*, 87-93.

9. Date, Y., Nakanishi, Y., Fukuda, S., Nuijima, Y., Kato, T., Umehara, M., Ohno, H., Kikuchi, J. (2014) In vitro evaluation method for screening of candidate prebiotic foods. *Food Chem. 152*, 251-260.